Time-dependent Pinning of Nanoblisters Confined by Two-dimensional Sheets. Part 1: Scaling Law and Hydrostatic Pressure

Chengfu Ma,[1,2,*] Yuhang Chen,[2,*] and Jiaru Chu[1,2]

[1] *CAS Key Laboratory of Mechanical Behavior and Design of Materials, Department of Precision Machinery and Precision Instrumentation, University of Science and Technology of China, Hefei 230026, China*

[2] *Key Laboratory of Precision Scientific Instrumentation of Anhui Higher Education Institutes, Department of Precision Machinery and Precision Instrumentation, University of Science and Technology of China, Hefei 230026, China*

(Dated: December 08, 2022)

ABSTRACT: Understanding the mechanics of blisters is important for studying two-dimensional (2D) materials, where nanoscale blisters appear frequently in their heterostructures. It also benefits understanding a novel partial wetting phenomenon, known as elastic-wetting, where droplets are confined by thin films. In this two-part work, we study the static mechanics of nanoscale blisters confined between a 2D elastic sheet and its substrate (Part 1), as well as their pinning/depinning dynamics (Part 2). Here, in Part 1, we investigate the morphology characteristics and hydrostatic pressures of the blisters by using atomic force microscopy (AFM) measurements and theoretical analysis. The morphology characteristics of the blisters are shown to be the interplay results of the elasticity of the capping sheet, the adhesion between the capping sheet and the substrate, and the interfacial tensions. A universal scaling law is observed for the blisters in the experiments. Our analyses show that the hydrostatic pressures inside the blisters can be estimated from their morphology characteristics. The reliability of such an estimation is verified by AFM indentation measurements of the hydrostatic pressures of a variety of blisters.

Keywords: blister; scaling law; hydrostatic pressure; atomic force microscopy; indentation

INTRODUCTION

Blisters form by the delamination in finite regions of a thin film from the substrate which it adheres to due to trapped liquids, gases or solid particles at the film-substrate interface. Examples of blisters can be widely seen both in nature and in engineering systems in a wide range of length scales. Recently, behaviors of blisters have attracted increasing attention owing to two main reasons. On the one hand, interfacial nanoscale blisters are found almost inevitable in van der Waals (vdW) heterostructures [1–4], that are stacks of different atomically thin two-dimensional (2D) materials. In spite of being detrimental for the functioning of vdW heterostructures which requires cleaning methods [1, 3–5], such blisters show promising benefits. For example, high hydrostatic pressures expected in such nanoblisters inspired studies of high-pressure-chemistry of confined molecules inside them [6, 7]. High strains in graphene nanoblisters were shown to be able to induce great pseudo–magnetic fields [8] and photoluminescence emitting [9]. On the other hand, blisters enclosing liquids represent a novel partial wetting phenomenon that stimulates research interests. In such a case, referred to as elastic-wetting elsewhere [10], the wetting behaviors of the confined droplets are governed together by the elasticity of the capping film and the surface tensions [10, 11].

Understanding the mechanics of blisters is therefore of great importance for both studies on 2D materials and wetting. A few studies have carried out theoretical analyses of the blister mechanics in equilibrium [2, 10, 12–14]. Universal scaling laws have been revealed for blisters confined by ultrathin films, which explained the characteristic aspect ratios (height-to-radius) or contact angles usually observed of 2D material blisters [2, 14–16]. The studies have also shown that the work of adhesion of a film to its substrate can be informed from the shape characteristics of blisters capped between them, so as the pressures inside the blisters [2, 12, 14]. However, quantitative measurements of such properties are still lacked to further verify the analyses. Moreover, while most studies focus on the equilibrium state of blisters, their dynamics have hardly been explored.

To this end, in this two-part work, we investigate both the static mechanics and dynamics of nanoscale blisters confined between a 2D elastic sheet and its substrate. Before we report our study on the pinning/depinning behaviors of such blisters in an accompanying paper (Part 2) [17], here in this part, which also serves as a basis to the analyses in Part 2, we investigate the morphology characteristics and hydrostatic pressures of the blisters. We first study the shape characteristics of the blisters by using atomic force microscopy (AFM) characterization and by a mechanics analysis. Then the hydrostatic pressures inside a variety of blisters are measured by AFM indentation tests, and compared with values estimated from their morphology characteristics to further verify the analysis.

* Corresponding authors: chfuma@ustc.edu.cn (C. M.); chenyh@ustc.edu.cn (Y. C.)

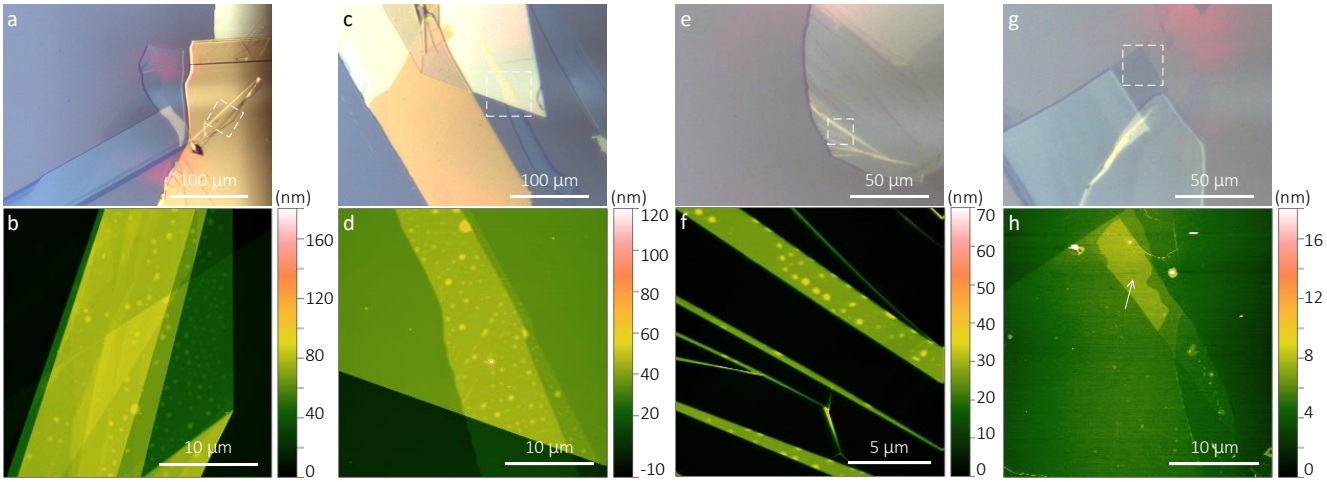

FIG. 1. Interfaces of different conditions. The optical images (upper) and the corresponding AFM topographies of the encased areas (lower) representing different interfaces. (a) (b) a folded graphite flake having a thickness of approx. 26.7 nm lying on another thicker graphite flake; (c) (d) an approx. 8.3 nm thick graphite strip with its upper part overlaying with another thicker graphite flake and its lower part lying on the SiO_2/Si substrate; (e) (f) an approx. 11.9 nm thick graphite flake on the SiO_2/Si substrate bearing folded strips; (g) (h) a double-layer graphene flake overlaid by a monolayer graphene strip.

EXPERIMENTAL SECTION

Sample Preparation. We study nanoscale blisters that are spontaneously formed between stacked thin graphite sheets. The sample was fabricated by using the Scotch Tape method [18], in which a tape is employed for mechanically exfoliating graphite and graphene flakes from a bulk graphite sample and then transferring them onto a substrate after repeat peeling. Here, the substrate is a SiO_2/Si wafer having an oxide layer thickness of 90 nm. The root mean square (RMS) roughness of the SiO_2/Si substrate was determined to be approx. 127 pm by AFM imaging. The sample was fabricated and kept in normal room temperature and humidity conditions.

Measurement Methods. All the AFM measurements were carried out on a commercial AFM (Dimension Icon, Bruker, CA). Its built-in camera was used for the optical imaging. The AFM topographies shown in Fig. 1 were obtained with a Multi75-G cantilever (Budget-Sensors, Bulgaria) in tapping mode. For all other AFM measurements, a RTESPA-525 probe (Bruker, CA) was used. The spring constant of the RTESPA-525 probe, which was used for the indentation measurements, was calibrated to be 218.2 N/m by using the Sader method [19]. Its tip was intentionally worn before the measurements by scanning on a sapphire sample in contact mode to avoid severe tip changes during the indentation tests due to wear or fracture. The curvature radius of its tip apex was measured to be approx. 82.8 nm after all the experiments by using a scanning helium ion microscope (ORION NanoFab, ZEISS). The thicknesses of graphite/graphene flakes are determined by measuring their step heights at their edges with AFM.

RESULTS AND DISCUSSION

Different interfaces and confined blisters. Spontaneously formed blisters are frequently observed between different 2D materials and their substrates [1–5, 14–16, 20]. Such blisters have typical lateral sizes from a few nanometers to micrometers, and may be formed through the aggregation of adsorbed molecules on the interface surfaces due to the vdW attraction between them. Although it's difficult to directly determine the substance inside the blisters, we conclude from the observation of residual wetting ridges after depinning the blisters (see Part 2 [17]) that for our sample it is at least liquid. Indeed, studies have suggested that absorbed liquid water is the most likely candidate rather than other possibilities of trapped air or hydrocarbon [1, 5, 14–16, 20, 21]. Especially, a study by Cao *et al* showed that the number density and the sizes of the nanoblisters are both reduced for graphene-graphite interfaces prepared at lower relative humidity [15]. Pizzocchero *et al* found that vdW heterostructures prepared at a high temperature of 110 °C result in complete absence of nanoblisters [1].

After a thorough investigation on many different interfaces, we find that confined blisters are observed only at interfaces of two overlaying graphite (or multilayer graphene) flakes. For instance, in Fig. 1 we show the optical and AFM topography images of some typical interfaces with different conditions. For the case in Figs. 1(a) and 1(b) where a folded graphite flake having a thickness of approx. 26.7 nm lays on another quite thick graphite flake, blisters can be seen being confined between them, but not at the interface between the underneath graphite flake and the SiO_2/Si substrate. This also applies in Figs. 1(c) and 1(d) where the upper part of an approx. 8.3 nm thick graphite strip overlays with another thicker graphite flake and its lower part lays on the SiO_2/Si substrate. Blisters can be observed between the graphite-graphite interface, but not at the both interfaces between the SiO_2/Si substrate and the graphite flakes. Blisters can also be seen at folding interfaces of graphite flakes, for example at the strip folding areas of

one graphite flake having a thickness of approx. 11.9 nm as shown in Figs. 1(e) and 1(f). Again, no blisters can be seen at the graphite-SiO_2/Si interface. Finally, we don't observe confined blisters between graphene (or few layer graphene) – graphene interfaces or graphene-SiO_2/Si interfaces. For example, Figs. 1(g) and 1(h) show a two-layer graphene flake and a monolayer graphene strip overlaying with each other. No blisters are seen at the graphene-SiO_2/Si interfaces or at the graphene-graphene interface. However, we occasionally observe layered features between graphene-graphene interfaces as the one indicated in Fig. 1(h) by an arrow. The interfacial layer has a thickness of approx. 1.2 nm. We suggest it to be a layer of water absorbed at the interface. Indeed, interfacial water adlayers confined by 2D materials on different substrates have previously been observed [22–24].

The formation mechanism of different interfacial structures under different interface conditions is not fully understood and is beyond the scope of this work. We suggest that it is an interplay result of the van der Waals (vdW) adhesion between the interfacing materials, the elastic properties of the capping layer, the surface tensions of the interfaces to the confined substances, as well as the interfacial roughness.

Morphology characteristics of the confined blisters. Next, we study the morphology characteristics of the blisters with AFM imaging. The study is carried out on blisters confined between two thin graphite flakes which form a triangular overlaying area as can be seen from the optical image in Fig. 2(a). AFM imaging at the overlaying area reveals confined blisters between the graphite-graphite interface as shown in Fig. 2(b). The thicknesses of the graphite flakes are determined to be approx. 6.4 nm (flake 1) and 8.9 nm (flake 2). By analyzing the morphology changes of wrinkles on both graphite flakes that extend to the overlaid area, we determine that flake 2 is on top of flake 1. A zoomed-in imaging as the one in Fig. 2(c) shows that the confined blisters are mostly in near round shapes, except a few elongated ones which indicate local anisotropic tensions in the capping sheet [11]. For example, blisters near wrinkles are seen to be elongated along the wrinkles' directions. For simplicity, our further study is carried out on a number of blisters that are relatively far from such wrinkles or other blemishes and have near round shapes. They are then treated as circularly symmetric without local anisotropic tensions in their capping sheets. The studied blisters are analyzed to have a small mean aspect ratio (major to minor axes) of $\sim$1.11$\pm$0.06 by using the quick shape fitting function of the Gwyddion software.

As can be seen from the AFM topography of a typical blister displayed in three dimension (3D) in Fig. 2(d), the studied blisters resemble spherical caps. To quantify their dimension characteristics, their center heights h and capping radii a, as illustrated in the inset of Fig. 2(d), are analyzed. To do so, the height profiles across their centers horizontally are first extracted from local AFM topography images of them. For example, we show in Fig. 2(e) typical height profiles representing blisters from the largest to the smallest. All the height profiles are then found to be well described with the assumed deflection of a pressurized membrane [12] as schematically shown in the inset of Fig. 2(d),

$$w(r) = h\left(1 - \frac{r^2}{a^2}\right), \tag{1}$$

where $w(r)$ is its deflection at a radial distance of r from the center. This can be seen from the good fittings acquired by Eq. (1) to all the blister's height profiles (see Fig. 2(e)). This indicates that the bulged capping sheets of the blisters behave as membranes.

Indeed, previous studies have shown an effective length scale $h_e \sim \sqrt{D/K}$,[12] or more precisely $h_e = \sqrt{12(1-\nu^2)D/K}$),[13] representing the ratio between the bending modulus and the in-plane stretching modulus. Here, $D = Et^3/12(1-\nu^2)$ is the flexural rigidity of the capping sheet, $K = E_{in}t$ is defined as its in-plane elastic stiffness, in which E and ν are respectively the Young's modulus and Poisson's ratio, E_{in} is its in-plane Young's modulus and t is its thickness. For a pressurized sheet, if its center height h is sufficiently larger than the length scale h_e, then it can be treated as a membrane. Otherwise, the effect of bending stiffness is no longer negligible and a plate theory should be considered. For common isotropic materials, $E = E_{in}$, we thus have $h_e = t$. This requires a central deflection that is several times larger than the sheet thickness to apply the membrane analysis [25]. However, as a lamellar material, graphite has different out-of-plane and in-plane Young's moduli [26]. Considering E=36.5 GPa, ν=0.16, E_{in}=1.06 TPa, [26] and the thickness $t \sim$8.9 nm, we have $h_e \sim$1.65 nm. Almost 87% of the blisters in our study have central deflections h that are at least 5 times larger than h_e, and even the smallest one has $h/h_e \sim$3.0. This suggests that the membrane analysis is applicable for them, and describing their deflections with Eq. (1) is expected to be accurate.

Then by fitting the blisters' height profiles with Eq. (1), their radii a and center heights h are obtained. It should be noted that the measured radii a contain slight tip convolution effects [27] which are deduced. In addition, as in Eq. (1) or in our further analysis, the radii of the blisters are defined from the middle plane of the capping sheet. Therefore, an additional correction to a is applied by subtracting half the sheet thickness $t/2$. The measured dimensional characteristics of the blisters after corrections are shown in Fig. 2(f). An almost linear relation between their center heights and radii, i.e. a constant aspect ratio $h/a \sim$0.062$\pm$0.003, is observed. Such a scaling law is indeed also observed elsewhere [2, 14–16] for blisters confined in various interfaces.

Scaling law analysis. To understand the observed scaling law, we conduct a mechanics analysis based on the theory of elasticity. For this purpose, we model the blisters as pressurized elastic sheets as illustrated in the

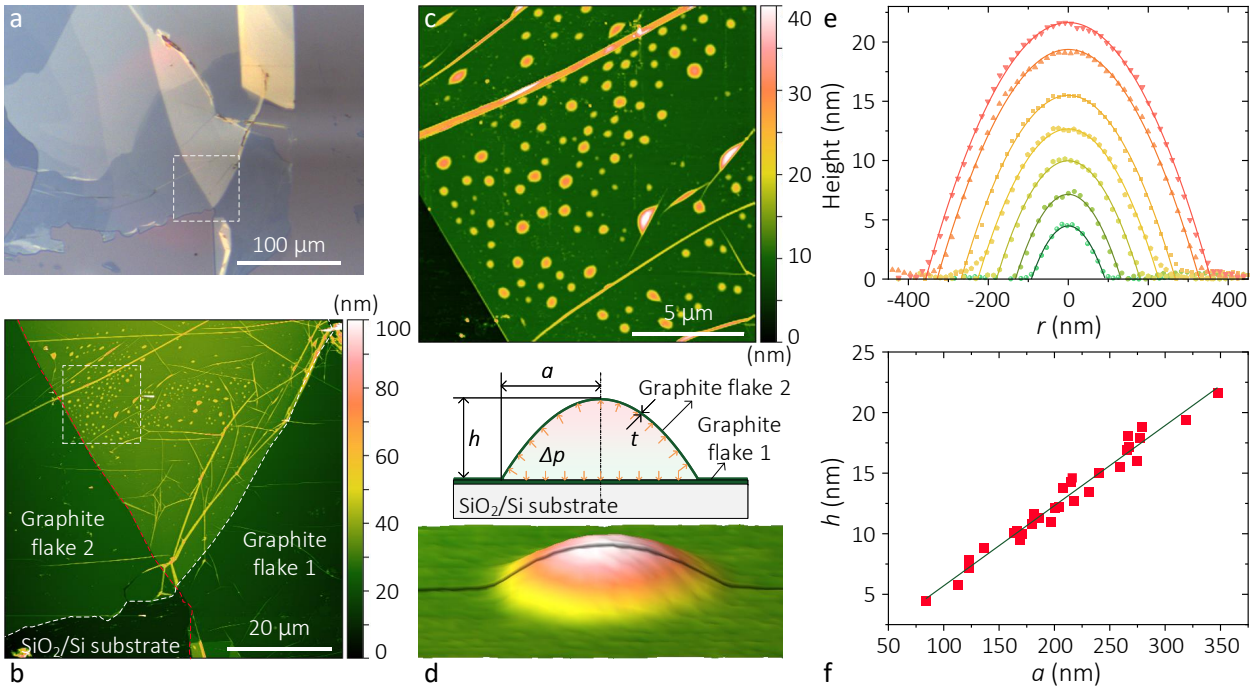

FIG. 2. **Shape characteristics of the blisters.** (a) Optical and (b) AFM topography images of two overlaying graphite flakes on a SiO_2/Si substrate; (c) AFM topography of the encased area in (b); (d) 3D display of AFM topography of a typical blister, and a schematic model of it (inset); (e) AFM measured height profiles across the centers of typical blisters (data points), fitted by the assumed deflections for pressurized membranes (lines); (f) The central heights h of all the measured blisters as a function of their radii a (data points), and a linear fit of the data (line).

inset of Fig. 2(d), with their deflections being described by Eq. (1). In addition, for the deformation to be kinematically admissible, we assume the radial displacement of the pressurized sheet inside the blister ($|r| \leq a$, indicated by the superscript '-') to be

$$u^-(r) = u_0 \frac{r}{a}\left(1 - \frac{r^2}{a^2}\right) + u_s \frac{r}{a}, \tag{2}$$

where u_0 is a parameter to be determined and u_s represents the radial displacement at the edge of the blister $r = a$. For a clamped edge, u_s=0. However, here we adopt a sliding boundary condition considering that the interlayer shear interaction between the graphite capping sheet and the graphite substrate may be weak [28, 29]. This permits radial displacements of the capping sheet both inside and outside the blisters, which can be considered as the Lamé problem. Taking account of the displacement continuity at the blister edge, we have for the radial displacement outside the blister ($|r| > a$, represented by the superscript '+')

$$u^+(r) = u_s \frac{a}{r}, \tag{3}$$

which approaches to 0 for a distance far enough $r \to \infty$.

The radial and circumferential strain components of the capping sheet in- and outside the bulging part are then obtained as

$$\begin{cases} \varepsilon_r^- = \dfrac{du^-}{dr} + \dfrac{1}{2}\left(\dfrac{dw}{dr}\right)^2 = \dfrac{u_0 + u_s}{a} - \dfrac{3u_0 r^2}{a^3} + \dfrac{2h^2 r^2}{a^4}, \\ \varepsilon_\theta^- = \dfrac{u^-}{r} = \dfrac{u_0 + u_s}{a} - \dfrac{u_0 r^2}{a^3}, \\ \varepsilon_r^+ = -\varepsilon_\theta^+ = -\dfrac{a u_s}{r^2}. \end{cases} \tag{4}$$

Additionally, the corresponding radial and circumferential tensile forces (membrane forces) per unit length are obtained as

$$\begin{cases} N_r^- = \sigma_r^- t = \dfrac{K}{1-\nu^2}(\varepsilon_r^- + \nu\varepsilon_\theta^-), \\ N_\theta^- = \sigma_\theta^- t = \dfrac{K}{1-\nu^2}(\varepsilon_\theta^- + \nu\varepsilon_r^-), \\ N_r^+ = -N_\theta^+ = \dfrac{K}{1-\nu^2}(1-\nu)\varepsilon_r^+. \end{cases} \tag{5}$$

where σ_r, σ_θ represent respectively the radial and circumferential stresses. Then, taking account the continuity of the radial stress at the blister edge, we derive

$$u_s = u_0 - \frac{h^2}{a}. \tag{6}$$

The total energy of the system is then a function of the three kinematic parameters a, h and u_0, and we further determine their relations by using the principle of

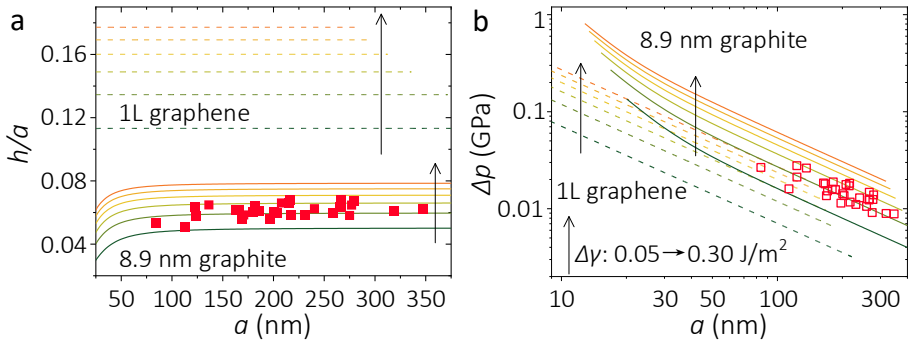

FIG. 3. The aspect ratios of blisters and their hydrostatic pressures inside. (a) The theoretical aspect ratio h/a and (b) the hydrostatic pressure Δp as functions of the radii a of blisters confined by a monolayer graphene (dotted line) and an 8.9 nm thick graphite sheet (solid line) for various $\Delta\gamma$ of 0.05, 0.10, 0.15, 0.20, 0.25 and 0.30 J/m^2. The measured ones for h/a and the calculated Δp from the measured dimensional quantities of the 8.9 nm thick graphite sheet are plotted as data points.

minimum energy at equilibrium. The total energy of the system can be written as

$$\begin{aligned}\Pi =& E_b^- + E_s^- + E_s^+ + \pi a^2\Delta\gamma - \Delta pV \\ =& 2\pi\int_0^a U_b^-(r)rdr + 2\pi\int_0^a U_s^-(r)rdr \\ &+ 2\pi\int_a^\infty U_s^+(r)rdr + \pi a^2\Delta\gamma - \Delta pV,\end{aligned} \tag{7}$$

where E_b^- represents the bending energy of the bulging part of the sheet, E_s^- and E_s^+ are respectively its stretching energies in- and outside the blister, and U_b^-, U_s^-, and U_s^+ are respectively the corresponding energies per unit area, which can be derived by

$$\begin{cases} U_b(r) = \dfrac{D}{2}\left[\left(\dfrac{d^2w}{dr^2}\right)^2 + \dfrac{1}{r^2}\left(\dfrac{dw}{dr}\right)^2 + \dfrac{2\nu}{r}\dfrac{dw}{dr}\dfrac{d^2w}{dr^2}\right], \\ U_s(r) = \dfrac{K}{2(1-\nu^2)}(\varepsilon_r^2 + 2\nu\varepsilon_r\varepsilon_\theta + \varepsilon_\theta^2). \end{cases} \tag{8}$$

The term $\pi a^2\Delta\gamma$ in Eq. (7) corresponds to the energy associated with separating the capping sheet from the substrate by the blister substance, where $\Delta\gamma = \gamma_{cb}+\gamma_{sb}-\gamma_{cs}$, and γ_{cb}, γ_{sb}, γ_{cs} represent the interfacial tensions between the capping sheet ('c'), the blister substance ('b'), and the substrate ('s'). The last term represents the free energy of the substance inside the blister where Δp is the hydrostatic pressure and $V = \pi a^2 h/2$ is its volume.

By applying the integrals in Eq. (7), and considering the blister to be in equilibrium with a fixed radius a, we derive u_0 from the principle of minimum free energy which requires $\left(\frac{\partial\Pi}{\partial u_0}\right)_a = 0$ as

$$u_0 = \frac{3-\nu}{4}\frac{h^2}{a}. \tag{9}$$

Additionally, from $\left(\frac{\partial\Pi}{\partial a}\right)_V = 0$ and $\left(\frac{\partial\Pi}{\partial V}\right)_a = 0$, $\Delta\gamma$ and Δp can be determined as

$$\Delta\gamma = 12(1+\nu)D\frac{h^2}{a^4} + \frac{5}{6}K\frac{h^4}{a^4}, \tag{10}$$

$$\Delta p = 16(1+\nu)D\frac{h}{a^4} + \frac{4}{3}K\frac{h^3}{a^4}. \tag{11}$$

It can be seen that the right-hand sides of both Eqs. (10) and (11) are composed of a term due to bending and a term due to stretching. If we consider the capping sheet as a pure membrane, the contribution from the bending energy and thus the first terms can be ignored. This yields a relation of $\Delta\gamma = \frac{5}{6}K\frac{h^4}{a^4}$, which indeed implies a constant aspect ratio h/a determined together by $\Delta\gamma$ and K. Where the capping sheet can no longer be considered as a membrane, but rather a plate, the bending portion induces a nonlinear effect on the aspect ratio that depends on the blister size.

In Fig. 3(a), we show calculations of h/a as a function of the blister radius for the 8.9 nm thick graphite sheet according to Eq. (10) by assuming different $\Delta\gamma$. For comparison, calculations are also done for the case of a monolayer graphene as the capping layer, where a thickness of t=0.345 nm is used. It can be found that for monolayer graphene which can be considered as a pure membrane, a universal scaling can be observed. For the graphite sheet, which consists of ∼26 atomic layers, however, a constant aspect ratio can only be found for blisters with radii larger than about ∼100 nm. For a smaller blister, the contribution of the bending portion in the capping layer arises gradually and this leads to nonlinear dependence of h/a on the blister radius. By also plotting the experimentally measured aspect ratios in Fig. 3(a), we can see that most of the data are in the membrane range which agrees with our discussion before. In addition, the generally constant aspect ratio meets the theoretical expectation.

From the linear relation between $\Delta\gamma$ and $(h/a)^4$ for membrane consideration, it can be seen that by knowing the aspect ratio, $\Delta\gamma$ can be determined. Here, from the measured h/a values in our experiments, we obtain $\Delta\gamma \sim 0.117\pm0.025$ J/m^2. Furthermore, considering the classical Young–Dupré equation, we generate the adhesion energy Γ between the capping sheet and the substrate as

$$\Gamma = \Delta\gamma + \gamma_b(\cos\theta_c + \cos\theta_s), \tag{12}$$

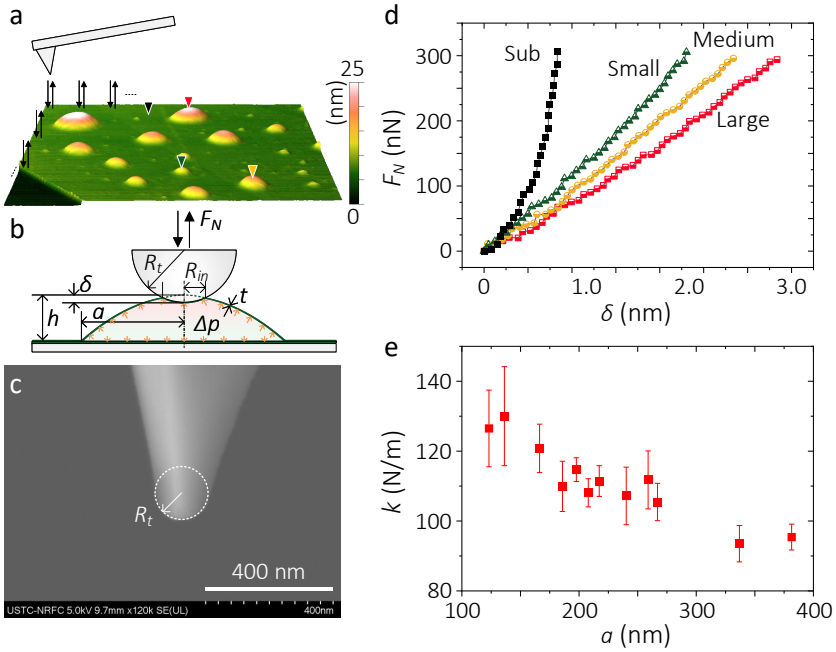

FIG. 4. Indentation of the blisters by AFM. (a) Illustration of volume force curve measurement by AFM and the 3D display of the simultaneously acquired topography; (b) Schematic illustration of the indentation at the center of a blister; (c) SEM image of the tip apex; (d) Example force-displacement curves acquired at the centers of respectively a large, a medium and a small blister, and at the graphite substrate; (e) The indentation stiffnesses of blisters as functions of their radii.

where γ_b is the surface tension of the substance in blister, θ_c and θ_s are respectively its contact angles on the capping and substrate materials in air. This means that the adhesion energy of a 2D material to its substrate can be estimated from the aspect ratios of spontaneously confined blisters between them, with the knowledge of the elastic properties of the 2D material, its thickness, and the interfacial tensions. This no doubt provides a simple alternative to the artificial blister test [30, 31]. Here, for our experiments, if we consider water as the confined substance whose surface tension and contact angle on graphite are taken [32] as $\gamma_b \sim 0.072$ J/m^2, $\theta_c = \theta_s = \theta_g \sim 90.6°$, then the adhesion energy between the graphite-graphite interface is estimated to be 0.115 ± 0.025 J/m^2.

In addition to the adhesion energy, another important information, i.e. the hydrostatic pressure Δp inside a blister, can be inferred from the model (Eq. 11). In Fig. 3(b) we show the theoretical Δp as a function of the blister radius a for both a monolayer graphene and the 8.9 nm thick graphite sheet under various $\Delta\gamma$. The values calculated according to Eq. (11) are also given for the blisters in our experiments. It can be seen that Δp increases by a power law with reducing the blister size. For the blisters in this study, their inner pressures are of ~ 9 MPa for the largest blister with a radius of ~ 350 nm and can reach as high as ~ 28 MPa for blisters as small as ~ 100 nm in radii. In fact, there have been attempts of studying chemical reactions of confined molecules in even smaller graphene blisters by taking advantage of the high-pressure conditions inside [6, 7]. Pressures as high as 1 GPa can be reached inside graphene blisters as small as a few nanometers in radii, which can even etch the diamond surface [20].

Hydrostatic pressure measurement by AFM indentation. To further verify our analysis above, here we report our measurements of the hydrostatic pressures inside the blisters. We first measure their load-displacement responses by AFM indentation. Then the hydrostatic pressures are estimated by comparing the measurements to a solution of the Föppl–von-Karman (FvK) equation that describes the indentation of a pressurized membrane [33].

The measurements are performed on the same sample as in Fig. 2 in a zoom-in area. To avoid the problem of scan drift which makes positioning to the exact centers of the blisters challenging, especially for smaller ones, a so-called force volume measurement is employed. By doing so, force-distance curves are collected point-by-point in a 200×200 grid over the full 4×4 μm^2 scan area, and a topography is simultaneously acquired as shown in Fig. 4(a). Then those force curves at the blisters' centers are extracted and analyzed afterwards. The indentation of a blister by an AFM tip is illustrated in Fig. 4(b), where the blister is deformed by a central displacement of δ by the tip load of F_N. It should be mentioned that the AFM tip has a radius of approx. $R_t \sim 82.8$ nm, as measured by its SEM imaging after all the measurements as shown in Fig. 4(c). However, the actual loading area should be much smaller as illustrated in Fig. 4(b) by the radius

R_{in}, which we will discuss later.

The central force-displacement ($F_N \sim \delta$) curves of a number of blisters are analyzed whose sizes span from $a \sim$ 120 nm to $a \sim 380$ nm. Example results are displayed in Fig. 4(d) of three blisters having radii a of 336.8 nm (large), 207.8 nm (medium) and 136.3 nm (small), and of the graphite substrate, as marked in Fig. 4(a). Unlike the clearly nonlinear indentation curve on the substrate, it can be seen that the $F_N \sim \delta$ curves on the blisters are near linear. In addition, it can be found that smaller blisters show stiffer responses to indentation, with smaller displacements for the same loading. To reveal such a behavior more clearly, we define a parameter k representing the "indentation stiffness" of a blister which is the slope of its $F_N \sim \delta$ curve obtained from a linear fitting. For all the measured blisters, nine force curves at the center are analyzed. In Fig. 4(e), the resulting mean values of k with their standard deviations are shown for the blisters as functions of their radii. An increase of the indentation stiffness can be seen unambiguously for smaller blisters. This indicate a larger hydrostatic pressure Δp inside a smaller blister as expected by our analysis before. However, a further analysis is need to quantify Δp from the $F_N \sim \delta$ curves.

A previous study [34] indeed predicts a linear relationship between the loading force and the displacement while indenting a pressurized elastic shell by a point force. In the case of indenting a pressurized membrane having a capping radius of a with an indenter with finite size, Vella and Davidovitch [33] have found that the force-displacement relationship $F_N \sim \delta$ follows

$$F_N = 2\pi T_{eff}\delta / \log \frac{a}{R_{in}}, \tag{13}$$

in the regime of small relative displacement, $\tilde{\delta} = \delta/h \ll 1$. Here, T_{eff} is the pressurization-induced tension at the center of the bulging membrane which is close to the indentation point. For large indentation $\tilde{\delta} \gg 1$, an additional nonlinear term $F_N \propto \delta^3$ should be included. The near linear relationships observed in our experiments clearly meet the signature of being in the small indentation regime [33]. For all the measured blisters in this study, the maximum indentations $\tilde{\delta}$, that are reached under a maximum load of ~ 300 nN, are determined to be in a range over from $\sim 14\%$ of the largest one to $\sim 30\%$ of the smallest one. However, to further ensure the small indentation condition, our future analyses are carried out on parts of the $F_N \sim \delta$ curves that are below $\tilde{\delta} \sim 10\%$.

From Eq. (13), it can be seen that for a specific indenting size R_{in}, the $F_N \sim \delta$ curve results in a constant indentation stiffness $k = 2\pi T_{eff}/\log \frac{a}{R_{in}}$. Thus, by measuring this stiffness k of a blister, and by knowing its capping radius a and the radius of the loading area R_{in}, the pressurization-induced tension T_{eff} can be estimated from which the inner pressure Δp can be determined. Unfortunately, in the case of AFM indentation, R_{in} is hardly known. In addition, AFM probes often possess non-flat tip apex as the round one in our case

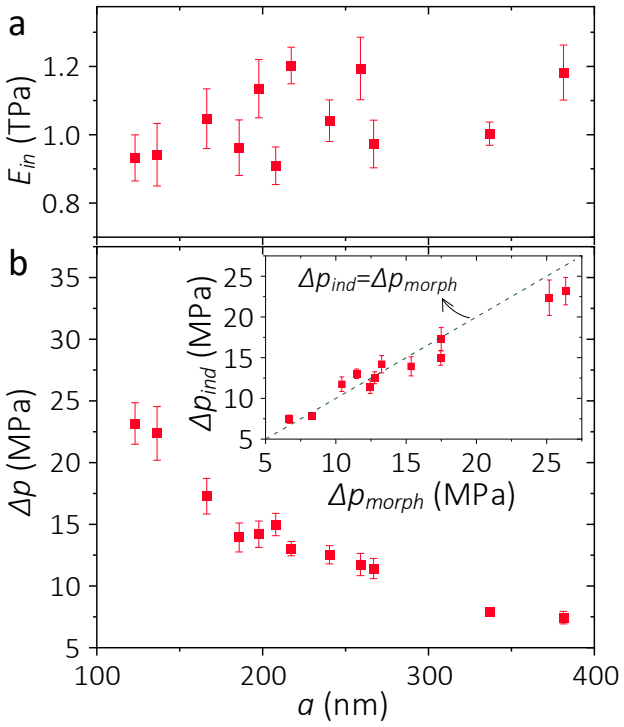

FIG. 5. Hydrostatic pressures inside blisters measured from AFM indentation tests. (a) The in-plane modulus E_{in} and (b) the hydrostatic pressures Δp of blisters estimated from their indentation tests. The hydrostatic pressures measured by indentation tests (Δp_{ind}) and the ones informed from the blisters' morphology characteristics (Δp_{morph}) are compared in the inset of (b).

(Fig. 4(c)), this results in a R_{in} changing with δ, as illustrated in Fig. 4(b). Therefore, we take this effect into account in our analysis rather than using a fixed value for R_{in}. Considering that the studied blisters' curvature radii $R \sim a^2/2h$ is much larger than the tip radius R_t, we derive $R_{in} \sim \sqrt{2R_t\delta}$ from a geometric simplification. Then, we fit all the $F_N \sim \delta$ curves with Eq. (13) and obtain the T_{eff} of all the blisters.

From our scaling analysis, we have the pressurization-induced tension at the blister center (see Eq. (5)) as

$$T_{eff} = \frac{N_r^-(0) + N_\theta^-(0)}{2} = \frac{K}{2}\frac{h^2}{a^2}. \tag{14}$$

This indicates that the in-plane stiffness $K = E_{in}t$ of the capping sheet and further its in-plane Young's modulus E_{in} can be informed from the measured T_{eff}. In Fig. 5(a), we show the resulting E_{in} by such a method. The results reveal a mean value of $E_{in} \sim 1044 \pm 108$ GPa, which is quite close to the adopted value [26] of 1.06 TPa in our scaling law analysis.

In addition, we have from the scaling analysis that $\Delta p = \frac{4}{3}K\frac{h^3}{a^4}$ in the membrane regime (see Eq. (11)). By combining with Eq. (14), this then leads to

$$\Delta p = \frac{8}{3}T_{eff}\frac{h}{a^2}. \tag{15}$$

From the measured T_{eff} values, the hydrostatic pressures inside the blisters can then be determined as shown in Fig. 5(b). A clear increase of the hydrostatic pressure can be seen with decreasing the blister size, from ~ 7.4 MPa for the largest blister with $a \sim 381$ nm to ~ 23.2 MPa for the smallest one with $a \sim 123$ nm. This agrees with our discussion in the scaling law analysis, see Fig. 3(b). More clearly, in the inset of Fig. 5(b), we compare the measured hydrostatic pressures of the blisters from the indentation tests (Δp_{ind}) to the ones informed directly from their morphology characteristics a and h by using Eq. (11) (Δp_{morph}). It can be seen that the two results coincide considerably well, with a mean deviation of $\sim 9\%$. This indicates the validity of our scaling law analysis, and that the hydrostatic pressure inside a blister can be well informed from its morphology characteristics by additional knowing the elastic properties and thickness of its capping sheet.

CONCULSION

In summary, we have investigated the morphology characteristics and hydrostatic pressures of nanoscale blisters confined onto the substrate by a 2D material sheet. We conclude that the morphology characteristics of the blisters are the interplay results of the elasticity of the capping sheet, the adhesion between the capping sheet and the substrate, and the interfacial tensions. A universal scaling law was observed for the studied blisters in the experiments, though its break-down is expected by our analysis for blisters in the plate regime. Our analyses showed that by knowing the elastic properties of the capping sheet, the hydrostatic pressures inside the blisters can be estimated from their morphology characteristics. With additional knowledge of the interfacial tensions, the work of adhesion between the capping sheet and the substrate can be determined as well. The reliability of such estimations was verified by AFM indentation measurements of the hydrostatic pressures inside a variety of blisters which yields results that agree considerably well with values estimated from their morphology characteristics.

ACKNOWLEDGMENTS

This work was supported by the National Natural Science Foundation of China (No. 52005476, 52075517) and the Hefei Municipal Natural Science Foundation (No. 2021014). We thank the USTC Center for Micro- and Nanoscale Research and Fabrication for technical support.

DATA AVAILABILITY

Data supporting the findings of this study are available from the corresponding author upon reasonable request.

CONFLICT OF INTEREST

The authors declare no competing financial interest.

REFERENCES

[1] F. Pizzocchero, L. Gammelgaard, B. S. Jessen, J. M. Caridad, L. Wang, J. Hone, P. Bøggild, and T. J. Booth, The hot pick-up technique for batch assembly of van der Waals heterostructures. *Nature Communications*, **7**, 11894 (2016).

[2] E. Khestanova, F. Guinea, L. Fumagalli, A. K. Geim, and I. V. Grigorieva, Universal shape and pressure inside bubbles appearing in van der Waals heterostructures. *Nature Communications*, **7**, 12587 (2016).

[3] D. G. Purdie, N. M. Pugno, T. Taniguchi, K. Watanabe, A. C. Ferrari, and A. Lombardo, Cleaning interfaces in layered materials heterostructures. *Nature Communications*, **9**, 5387 (2018).

[4] M. R. Rosenberger, H. J. Chuang, K. M. McCreary, A. T. Hanbicki, S. V. Sivaram, and B. T. Jonker, Nano-"squeegee" for the creation of clean 2D material interfaces. *ACS Applied Materials & Interfaces*, **10**(12), 10379-10387 (2018).

[5] Y. Hou, Z. Dai, S. Zhang, S. Feng, G. Wang, L. Liu, Z. Xu, Q. Li, and Z. Zhang, Elastocapillary cleaning of twisted bilayer graphene interfaces. *Nature Communications*, **12**, 5069 (2021).

[6] C. H. Y. X. Lim, M. Nesladek, and K. P. Loh, Observing High-Pressure Chemistry in Graphene Bubbles. *Angewandte Chemie International Edition*, **53**(1), 215-219 (2014).

[7] K. S. Vasu, E. Prestat, J. Abraham, J. Dix, R. J. Kashtiban, J. Beheshtian, J. Sloan, P. Carbone, M. Neek-Amal, S. J. Haigh, A. K. Geim, and R. R. Nair, Van der Waals pressure and its effect on trapped interlayer molecules. *Nature communications*, **7**, 12168 (2016).

[8] N. Levy, S. A. Burke, K. L. Meaker, M. Panlasigui, A. Zettl, F. Guinea, A. H. Castro Neto, M. F. Crommie, Strain-induced pseudo–magnetic fields greater than 300 tesla in graphene nanobubbles. *Science*, **329**(5991), 544-547 (2010).

[9] A. V. Tyurnina, D. A. Bandurin, E. Khestanova, V. G. Kravets, M. Koperski, F. Guinea, A. N. Grigorenko, A. K. Geim, and I. V. Grigorieva, Strained bubbles in van der Waals heterostructures as local emitters of photoluminescence with adjustable wavelength. *ACS photonics*, **6**(2), 516-524 (2019).

[10] Y. Rao, S. Qiao, Z. Dai, and N. Lu, Elastic wetting: Substrate-supported droplets confined by soft elastic membranes. *Journal of the Mechanics and Physics of Solids*, **151**, 104399 (2021).

[11] R. D. Schulman, and K. Dalnoki-Veress, Droplets capped with an elastic film can be round, elliptical, or nearly square. *Physical Review Letters*, **121**(24), 248004 (2018).

[12] K. Yue, W. Gao, R. Huang, and K. M. Liechti, Analytical methods for the mechanics of graphene bubbles. *Journal of Applied Physics*, **112**(8), 083512 (2012).

[13] P. Wang, W. Gao, Z. Cao, K. M. Liechti, and R. Huang, Numerical analysis of circular graphene bubbles. *Journal of Applied Mechanics*, **80**(4), 040905 (2013).

[14] D. A. Sanchez, Z. Dai, P. Wang, A. Cantu-Chavez, C. J. Brennan, R. Huang, and N. Lu, Mechanics of spontaneously formed nanoblisters trapped by transferred 2D crystals. *Proceedings of the National Academy of Sciences*, **115**(31), 7884-7889 (2018).

[15] P. Cao, K. Xu, J. O. Varghese, and J. R. Heath, The microscopic structure of adsorbed water on hydrophobic surfaces under ambient conditions. *Nano Letters*, **11**(12), 5581-5586 (2011).

[16] M. Cheng, D. Wang, Z. Sun, J. Zhao, R. Yang, G. Wang, W. Yang, G. Xie, J. Zhang, P. Chen, C. He, D. Liu, L. Xu, D. Shi, E. Wang, and G. Zhang, A route toward digital manipulation of water nanodroplets on surfaces. *ACS Nano*, **8**(4), 3955-3960 (2014).

[17] C. Ma, Y. Chen, and J. Chu, Time-dependent pinning of nanoblisters confined by two-dimensional sheets. Part 2: contact line pinning. *Langmuir*, submitted.

[18] K. S. Novoselov, A. K. Geim, S. V. Morozov, D. Jiang, Y. Zhang, S. V. Dubonos, I. V. Grigorieva, and A. A. Firsov, Electric field effect in atomically thin carbon films. *Science*, **306**(5696), 666-669 (2004).

[19] J. E. Sader, J. A. Sanelli, B. D. Adamson, J. P. Monty, X. Wei, S. A. Crawford, J. R. Friend, I. Marusic, P. Mulvaney, and E. J. Bieske, Spring constant calibration of atomic force microscope cantilevers of arbitrary shape. *Review of Scientific Instruments*, **83**(10), 103705 (2012).

[20] C. H. Y. X. Lim, A. Sorkin, Q. Bao, A. Li, K. Zhang, M. Nesladek, and K. P. Loh, A hydrothermal anvil made of graphene nanobubbles on diamond. *Nature Communications*, **4**, 1556 (2013).

[21] M. J. Lee, J. S. Choi, J. S. Kim, I. S. Byun, D. H. Lee, S. Ryu, C. Lee and B. H. Park, Characteristics and effects of diffused water between graphene and a SiO2 substrate. *Nano Research*, **5**(10), 710-717 (2012).

[22] K. Xu, P. Cao, and J. R. Heath, Graphene visualizes the first water adlayers on mica at ambient conditions. *Science*, **329**(5996), 1188-1191 (2010).

[23] H. Komurasaki, T. Tsukamoto, K. Yamazaki, and T. Ogino, Layered structures of interfacial water and their effects on Raman spectra in graphene-on-sapphire systems. *The Journal of Physical Chemistry C*, **116**(18), 10084-10089 (2012).

[24] Q. Li, J. Song, F. Besenbacher, M. Dong, Two-dimensional material confined water. *Accounts of Chemical Research*, **48**(1), 119-127 (2015).

[25] E. Ventsel, and T. Krauthammer, Thin Plates and Shells: Theory, Analysis, and Applications (Marcel Dekker, 2001).

[26] O. L. Blakslee, D. G. Proctor, E. J. Seldin, G. B. Spence, and T. Weng, Elastic constants of compression-annealed pyrolytic graphite. *Journal of Applied Physics*, **41**(8), 3373-3382 (1970).

[27] J. Canet-Ferrer, E. Coronado, A. Forment-Aliaga, and E. Pinilla-Cienfuegos, Correction of the tip convolution effects in the imaging of nanostructures studied through scanning force microscopy. *Nanotechnology*, **25**(39), 395703 (2014).

[28] Z. Liu, J. Yang, F. Grey, J. Z. Liu, Y. Liu, Y. Wang, Y. Yang, Y. Cheng, and Q. Zheng, Observation of microscale superlubricity in graphite. *Physical Review Letters*, **108**(20), 205503 (2012).

[29] G. Wang, Z. Dai, Y. Wang, P. Tan, L. Liu, Z. Xu, Y. Wei, R. Huang, and Z. Zhang, Measuring interlayer shear stress in bilayer graphene. *Physical Review Letters*, **119**(3), 036101 (2017).

[30] J. Chopin, D. Vella, and A. Boudaoud, The liquid blister test. *Proceedings of the Royal Society A: Mathematical, Physical and Engineering Sciences*, **464**(2099), 2887-2906 (2008).

[31] S. P. Koenig, N. G. Boddeti, M. L. Dunn, and J. S. Bunch, Ultrastrong adhesion of graphene membranes. *Nature Nanotechnology*, **6**(9), 543-546 (2011).

[32] J. Rafiee, X. Mi, H. Gullapalli, A. V. Thomas, F. Yavari, Y. Shi, P. M. Ajayan, and N. A. Koratkar, Wetting transparency of graphene. *Nature Materials*, **11**(3), 217-222 (2012).

[33] D. Vella, and B. Davidovitch, Indentation metrology of clamped, ultra-thin elastic sheets. *Soft Matter*, **13**(11), 2264-2278 (2017).

[34] D. Vella, A. Ajdari, A. Vaziri, A. Boudaoud, The indentation of pressurized elastic shells: from polymeric capsules to yeast cells. *Journal of the Royal Society Interface*, **9**(68), 448-455 (2012).

Abstract Graphics for Part 1